Magnesioreduction synthesis (Co-doped) β-$FeSi_2$: mechanism, microstructure and improved thermoelectric properties: supplementary information

Sylvain Le Tonquesse,[†] Zelia Verastegui,[†] Hélène Huynh,[‡] Vincent Dorcet,[†] Quansheng Guo,[‡,¶] Valérie Demange,[†] Carmelo Prestipino,[†] David Berthebaud,[‡] Takao Mori,[¶] and Mathieu Pasturel[*,†]

[†]*Univ Rennes, CNRS, ISCR-UMR6226/ScanMAT-UMS2001, F-35000, Rennes, France.*

[‡]*CNRS - Saint-Gobain - NIMS, UMI3629, Laboratory for Innovative Key Materials and Structures (LINK), National Institute for Materials Science, 1-1 Namiki, Tsukuba, Ibaraki 305-0044, Japan.*

[¶]*National Institute for Materials Science (NIMS), WPI-MANA and CFSN, Tsukuba, Japan.*

E-mail: mathieu.pasturel@univ-rennes1.fr

Phone: +33 (0)2 23 23 58 61

Abstract

β-$FeSi_2$ and β-$Co_{0.07}Fe_{0.93}Si_2$ thermoelectric silicides were synthesized from Fe_2O_3 and Si powders using a magnesiothermic process. Detailed study of the reaction mechanism by X-ray diffraction reveals that liquid Mg is mandatory to initiate the reduction. After completion of the reaction in relatively short time (10 h at 1173 K), the magnesiosynthesized iron disilicides are characterized as powders with grain sizes ranging

from 30 to 400 nm and containing a high concentration of stacking faults quantified for the first time using a dedicated refinement software. The thermoelectric properties of spark plasma sintered pellets with submicrometric grain sizes, high stacking fault density and residual micro- to nanoporosities are presented and compared to corresponding materials synthesized by conventional arc-melting process. Strong thermal conductivity reduction of 20 % at 773 K has been achieved thanks to the mesostructuration induced by the magnesioreduction. It results in an improved maximum figure-of-merit ZT reaching 0.18 at 773 K for β-$Co_{0.07}Fe_{0.93}Si_2$.

Keywords

Iron silicide, Thermoelectrics, Magnesiothermy, Mesostructuration, Stacking faults, Thermal conductivity

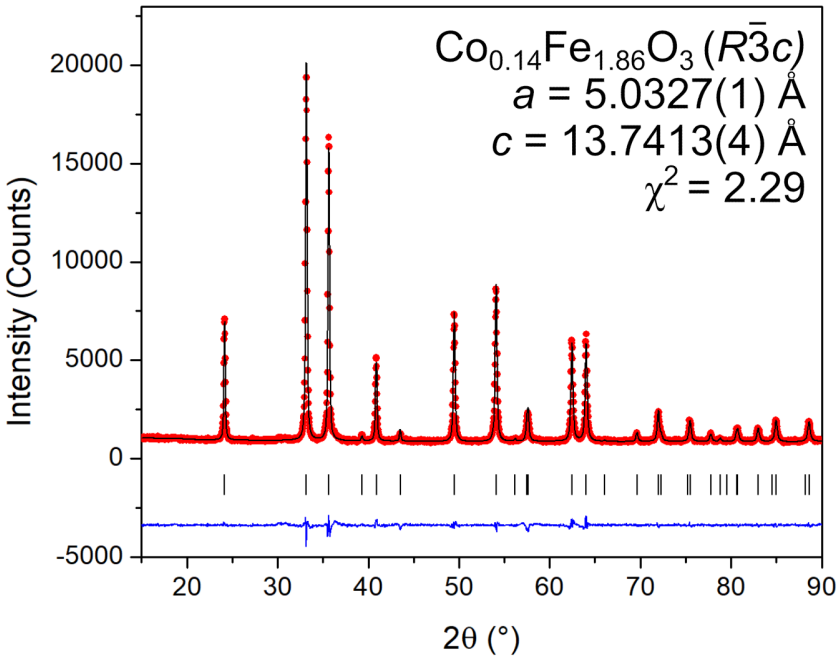

Figure S1: Le Bail refined powder XRD pattern of $Co_{0.14}Fe_{1.86}O_3$. The experimental data are plotted in red symbols, the calculated one in black line and the difference in blue line. The vertical ticks indicate the theoretical Bragg peak positions of Fe_2O_3.

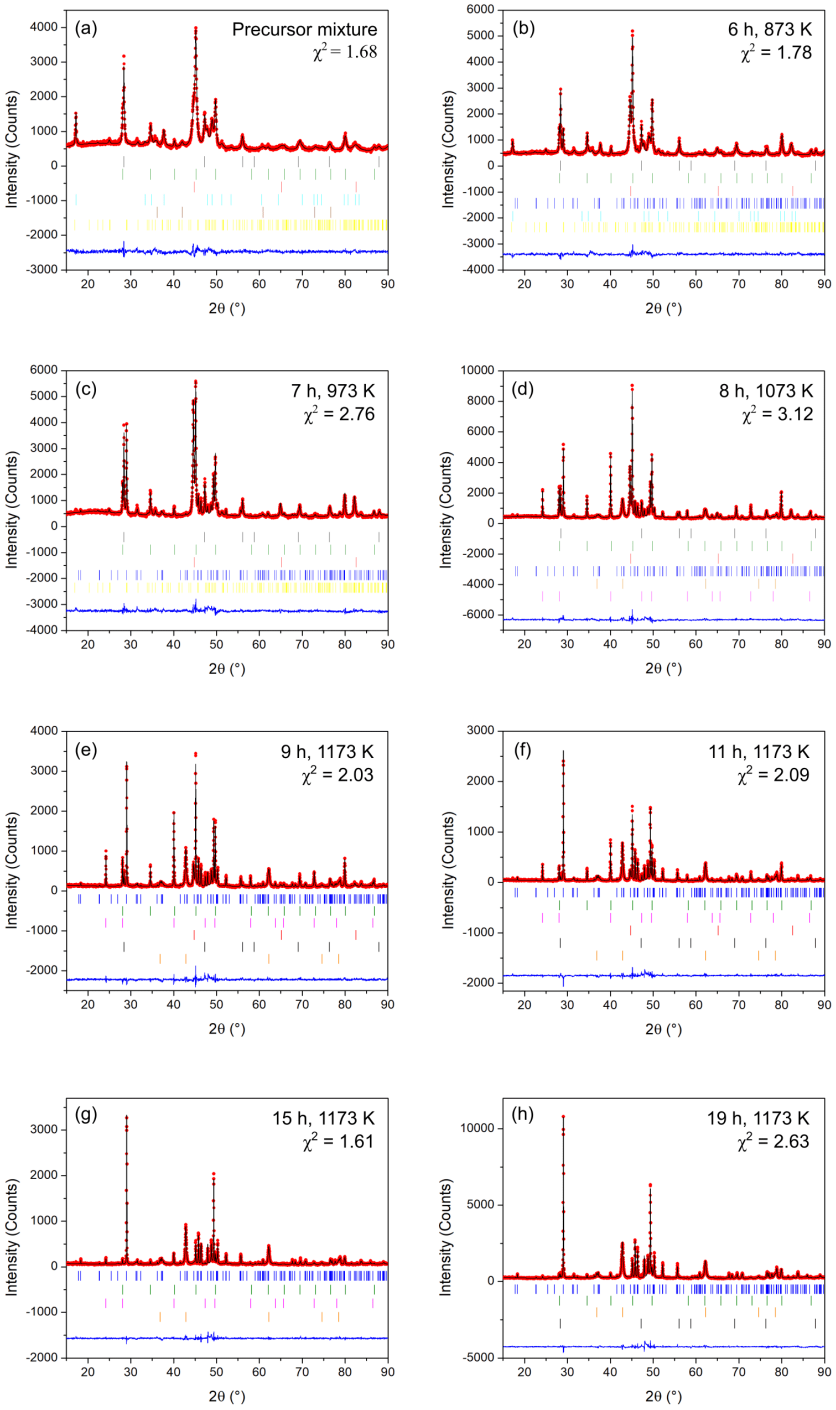

Figure S2: Rietveld refined XRD patterns of the magnesioreduced β-$FeSi_2$ samples at various stages of the reaction: the precursor mixture (a) and the reaction media after (b) 6 h, (c) 7 h, (d) 8 h, (e) 9 h, (f) 11 h, (g) 15 h and (h) 19 h. The experimental data are plotted in red symbols, the calculated one in black line and the difference in blue line. The vertical ticks indicate the theoretical Bragg peak positions for Si (black), Fe (red), FeSi (green), α-$Fe_{1-\delta}Si_2$ (bright blue), β-$FeSi_2$ (dark blue), FeO (purple), Mg_2Si (pink), Fe_2SiO_4 (yellow), MgO (orange).

Table S1: Structural parameters for β-$FeSi_2$ (s.g. *Cmce*) obtained from the Rietveld refinement of the XRD patterns in fig. S2. For patterns (a) to (f), the scale factor, lattice parameters and peak profile coefficients are the only refined parameters. The atomic coordinates are taken from Ref.[1] while the isotropic atomic displacement parameters are set to 0.2 Å^2 for Fe- and Si-atoms. For patterns (g) and (h), the atomic coordinates are refined and the peak shapes of the reflections fulfilling the condition k+l≠2n have been broadened using individual refined coefficients.

Pattern	a (Å)	b (Å)	c (Å)	Vol. Fraction (%)
(b)	9.921(3)	7.812(3)	7.835(3)	11(1)
(c)	9.912(1)	7.818(2)	7.830(1)	26(1)
(d)	9.9032(6)	7.8144(6)	7.8280(6)	26(1)
(e)	9.9000(5)	7.8131(5)	7.8267(5)	32(1)
(f)	9.8994(5)	7.8119(5)	7.8265(5)	41(1)
(g)	9.9007(4)	7.8098(4)	7.8291(4)	52(1)
(h)	9.8979(4)	7.8130(4)	7.8255(4)	54(1)

	Si (16g)			Si (16g)			Fe (8d)	Fe (8f)	
Pattern	x	y	z	x	y	z	x	y	z
(b)	0.1273	0.0450	0.2739	0.1282	0.2746	0.0512	0.2146	0.3086	0.3149
(c)	0.1273	0.0450	0.2739	0.1282	0.2746	0.0512	0.2146	0.3086	0.3149
(d)	0.1273	0.0450	0.2739	0.1282	0.2746	0.0512	0.2146	0.3086	0.3149
(e)	0.1273	0.0450	0.2739	0.1282	0.2746	0.0512	0.2146	0.3086	0.3149
(f)	0.1273	0.0450	0.2739	0.1282	0.2746	0.0512	0.2146	0.3086	0.3149
(g)	0.124(2)	0.043(2)	0.276(2)	0.126(2)	0.275(2)	0.0489(2)	0.216(1)	0.306(2)	0.311(2)
(h)	0.124(3)	0.042(3)	0.274(3)	0.127(3)	0.273(3)	0.051(3)	0.216(1)	0.309(2)	0.313(2)

Table S2: Structural parameters for Fe (s.g. $Im\bar{3}m$) obtained from the Rietveld refinement of the XRD patterns in fig. S2. The scale factor, lattice parameter and peak profile coefficients are the only refined parameters. The atomic coordinates are taken from Ref.[2] while the isotropic thermal displacement parameter is set to 0.3 Å^2.

Pattern	a (Å)	Vol. Fraction (%)	Fe (2a) x,y,z
(a)	2.8603(4)	17(1)	0
(b)	2.8681(3)	13(1)	0
(c)	2.8691(1)	19(1)	0
(d)	2.8694(2)	9(1)	0
(e)	2.867(1)	3(1)	0
(f)	2.867(1)	(2)	0

Table S3: Structural parameters for Si (s.g. $Fd\bar{3}m$) obtained from the Rietveld refinement of the XRD patterns in fig. S2. The scale factor, lattice parameter and peak profile coefficients are the only refined parameters. The atomic coordinates are taken from ref[3] while the isotropic thermal displacement parameter is set to 0.5 Å^2.

Pattern	a (Å)	Vol. Fraction (%)	Si ($8a$) x, y, z
(a)	5.435(4)	20(1)	1/8
(b)	5.4308(4)	16(1)	1/8
(c)	5.4304(3)	16(1)	1/8
(d)	5.431(1)	6(1)	1/8
(e)	5.431(1)	4(1)	1/8
(f)	5.430(1)	1(1)	1/8
(h)	5.431(1)	1(1)	1/8

Table S4: Structural parameters for FeSi (s.g. $P2_13$) obtained from the Rietveld refinement of the XRD patterns in fig. S2. The scale factor, lattice parameter and peak profile coefficients are the only refined parameters. The atomic coordinates are taken from Ref.[4] while the isotropic thermal displacement parameters are set to 0.2 Å^2 for Fe- and Si-atoms.

Pattern	a (Å)	Vol. Fraction (%)	Fe ($4a$) x,y,z	Si ($4a$) x,y,z
(a)	4.4813(4)	33(1)	0.3860	0.0917
(b)	4.4804(4)	39(1)	0.3860	0.0917
(c)	4.4849(5)	32(1)	0.3860	0.0917
(d)	4.4867(1)	26(1)	0.3860	0.0917
(e)	4.4851(2)	18(1)	0.3860	0.0917
(f)	4.4844(2)	12(1)	0.3860	0.0917
(g)	4.4839(2)	4(1)	0.3860	0.0917
(h)	4.4848(2)	4(1)	0.3860	0.0917

Table S5: Structural parameters for MgO (s.g. $Fm\bar{3}m$) obtained from the Rietveld refinement of the XRD patterns in fig. S2. The scale factor, lattice parameter and peak profile coefficients are the only refined parameters. The atomic coordinates are taken from Ref.[5] while the isotropic thermal displacement parameters are set to 0.3 Å^2 for Mg- and O-atoms.

Pattern	a (Å)	Vol. Fraction (%)	Mg ($4a$) x, y, z	O ($4b$) x, y, z
(c)	4.215(3)	1(1)	0	1/2
(d)	4.2134(4)	22(1)	0	1/2
(e)	4.2149(1)	31(1)	0	1/2
(f)	4.2152(3)	37(1)	0	1/2
(g)	4.2157(3)	40(1)	0	1/2
(h)	4.2160(6)	40(1)	0	1/2

Table S6: Structural parameters for Mg_2Si (s.g. $Fm\bar{3}m$) obtained from the Rietveld refinement of the XRD patterns in fig. S2. The scale factor, lattice parameter and coefficients for peak profile functions are the only refined parameters. The atomic coordinates are taken from Ref.[6] while the isotropic thermal displacement parameters are set to 0.3 Å^2 for Mg- and Si-atoms.

Pattern	a (Å)	Vol. Fraction (%)	Mg ($8c$) x,y,z	Si ($4a$) x,y,z
(d)	6.357(1)	12(1)	1/4	0
(e)	6.357(1)	12(1)	1/4	0
(f)	6.357(1)	8(1)	1/4	0
(g)	6.360(1)	4(1)	1/4	0
(h)	6.356(1)	1(1)	1/4	0

Table S7: Structural parameters for FeO (s.g. $Fm\bar{3}m$) obtained from the Rietveld refinement of the XRD patterns in fig. S2. The scale factor, lattice parameter and peak profile coefficients are the only refined parameters. The atomic coordinates are taken from Ref.[7] while the isotropic thermal displacement parameters are set to 0.3 Å^2 for Fe- and O-atoms.

Pattern	a (Å)	Vol. Fraction (%)	Fe ($4a$) x,y,z	O ($4b$) x,y,z
(a)	4.299(2)	3(1)	0	1/2

Table S8: Structural parameters for α-$FeSi_2$ (s.g. $P4/mmm$) obtained from the Rietveld refinement of the XRD patterns in fig. S2. The scale factor, lattice parameters and peak profile coefficients are the only refined parameters. The atomic coordinates are taken from Ref.[8] while the isotropic thermal displacement parameters are set to 0.3 Å^2 for Si- and Fe-atoms. Relative occupancy of the Fe ($1a$) position is set to 0.8.

Pattern	a (Å)	c (Å)	Vol. Fraction (%)	Fe ($1a$)[0.8] x,y,z	Si ($2h$) x,y	z
(a)	2.6855(4)	5.145(1)	19(1)	0	1/2	0.27
(b)	2.6882(6)	5.138(1)	10(1)	0	1/2	0.27

Table S9: Structural parameters for Fe_2SiO_4 (s.g. $Fd\bar{3}m$) obtained from the Rietveld refinement of the XRD patterns in fig. S2. The scale factor, lattice parameters and peak profile coefficients are the only refined parameters. The atomic coordinates are taken from Ref.[9] while the isotropic thermal displacement parameters are set to 0.3 Å^2 for Si-, Fe-atoms and 0.6 Å^2 for O-atoms.

Pattern	a (Å)	b (Å)	c (Å)	Vol. Fraction (%)
(a)	10.456(8)	6.141(8)	4.806(8)	7(1)
(b)	10.440(6)	6.112(6)	4.826(6)	11(1)
(c)	10.464(7)	6.110(7)	4.825(7)	6(1)

	Fe ($4a$)			Fe ($4c$)			Si ($4c$)		
Pattern	x	y	z	x	y	z	x	y	z
(a)	0	0	0	0.2286	1/4	0.5174	0.4108	1/4	0.072
(b)	0	0	0	0.2286	1/4	0.5174	0.4108	1/4	0.072
(c)	0	0	0	0.2286	1/4	0.5174	0.4108	1/4	0.072

	O ($4c$)			O ($4c$)			O ($8d$)		
Pattern	x	y	z	x	y	z	x	y	z
(a)	0.3981	1/4	0.7168	0.0358	1/4	0.2955	0.3080	0.0462	0.1931
(b)	0.3981	1/4	0.7168	0.0358	1/4	0.2955	0.3080	0.0462	0.1931
(c)	0.3981	1/4	0.7168	0.0358	1/4	0.2955	0.3080	0.0462	0.1931

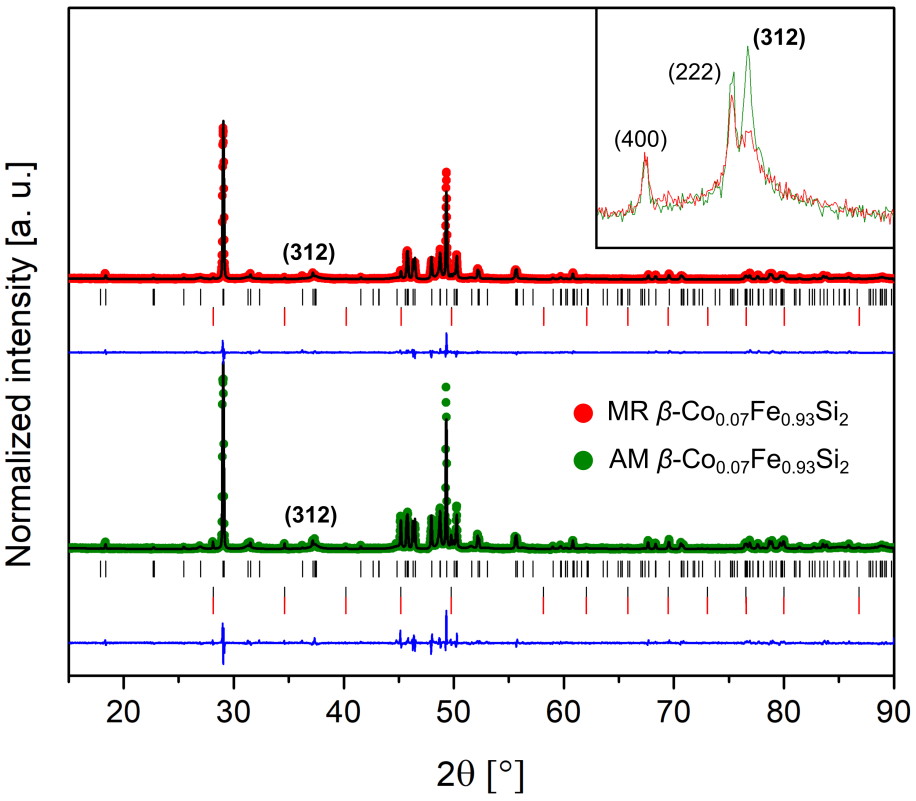

Figure S3: FAULTS refined powder XRD patterns of the sintered MR β-$Co_{0.07}Fe_{0.93}Si_2$ (red) and AM β-$Co_{0.07}Fe_{0.93}Si_2$ (green). The experimental data are plotted in colored symbols, the calculated one with a black line and the difference with a blue line. The vertical ticks indicate the Bragg peak positions for β-$FeSi_2$ (black) and FeSi (red). The inset is a close up view of the (312) reflections showing the different peak broadening between both samples.

Table S10: Lattice parameters, atomic coordinates, isotropic displacement parameters and stacking fault probability (SF) extracted from the Rietveld refinements of sintered MR and AM β-$FeSi_2$ and MR and AM β-$Co_{0.07}Fe_{0.93}Si_2$ XRD patterns.

		MR-$FeSi_2$	AM-$FeSi_2$	MR-$Co_{0.07}Fe_{0.93}Si_2$	AM-$Co_{0.07}Fe_{0.93}Si_2$
	a (Å)	9.89104(6)	9.87518(4)	9.91176(8)	9.91200(4)
	b (Å)	7.81612(4)	7.79980(3)	7.81410(4)	7.81500(4)
	c (Å)	7.84209(3)	7.83727(2)	7.84084(5)	7.84060(3)
	x	0.126(1)	0.126(1)	0.122(1)	0.122(1)
Si ($16g$)	y	0.046(1)	0.045(1)	0.045(1)	0.044(1)
	z	0.272(1)	0.274(1)	0.274(1)	0.274(1)
	x	0.129(1)	0.128(1)	0.130(1)	0.130(1)
Si ($16g$)	y	0.273(1)	0.275(1)	0.274(1)	0.274(1)
	z	0.049(1)	0.050(1)	0.048(1)	0.048(1)
Fe1 ($8f$)	y	0.308(1)	0.309(1)	0.307(1)	0.308(1)
	z	0.313(1)	0.313(1)	0.311(1)	0.311(1)
Fe2 ($8g$)	x	0.216(1)	0.216(1)	0.217(1)	0.217(1)
	SF (%)	10.7(2)	3.7(1)	10.4(1)	3.2(1)
	B_{iso} Fe (Å^2)	0.3(1)	0.4(1)	0.6(1)	0.2(1)
	B_{iso} Si (Å^2)	0.1	0.1(1)	0.4(1)	0.1(1)

References

(1) Dusausoy, P.; Protas, J.; Wandji, R.; Roques, B. Crystal structure of iron disilicide, $FeSi_2\beta$. *Acta Crystallogr. B* **1971**, *27*, 1209–1218.

(2) Zwell, L.; Speich, G.; Leslie, W. C. Effects of Co, Cr, Ir, Pt, Re, Rh, and Ru on lattice-parameter and density of α-iron. *Metall. Trans.* **1973**, *4*, 1990–1992.

(3) Dismukes, J.; Ekstrom, L.; Paff, R. Lattice parameters + density in germanium-silicon alloys. *J. Phys. Chem.* **1964**, *68*, 3021–3027.

(4) Weitzer, F.; Schuster, J. C. Phase-diagrams of the ternary-systems Mn, Fe, Co, Ni-Si-N. *J. Solid State Chem.* **1987**, *70*, 178–184.

(5) Wechsler, B. A.; Navrotsky, A. Thermodynamics and structural chemistry of compounds in the system MgO-TiO_2. *J. Solid State Chem.* **1984**, *55*, 165–180.

(6) Barlock, J. G.; Mondolfo, L. F. . Structure of some aluminium-iron-magnesium-manganese-silicon alloys. *Z. Metallkd.* **1975**, *66*, 605–611.

(7) Katsura, T.; Iwasaki, B.; Kimura, S.; Akimoto, S. High-pressure synthesis of stoichiometric compound FeO. *J. Chem. Phys.* **1967**, *47*, 4559–4560.

(8) Guéneau, C.; Servant, C. Quantitative determination of low phase volume fraction in ferrosilicon alloys by the Rietveld profile-refinement method. Neutron diffraction data compared with other methods. *J. Appl. Crystallogr.* **1995**, *28*, 707–716.

(9) Parker, S. C.; Catlow, C. R. A.; Cormack, A. N. Structure prediction of silicate minerals using energy-minimization techniques. *Acta Crystallogr. B* **1984**, *40*, 200–208.